Comprehensive Composite Inelastic Fiber Element for Cyclic Analysis of Concrete-Filled Steel Tube Columns

S. B. B. Aval[1]; M. A. Saadeghvaziri, M.ASCE[2]; and A. A. Golafshani[3]

Abstract: This paper presents the development of a comprehensive composite beam-column fiber element for large displacement nonlinear inelastic analysis of concrete-filled steel tube (CFT) columns. The bond/slip formulation represents the interaction between concrete and steel over the entire contact surface between the two materials. Thus, the modeling accounts for the two factors that cause the slippage between steel shell and concrete core. The first factor is the difference between axial elongation of the steel shell and the concrete core, and the second is the difference between curvatures in the cross section for the concrete core and the steel shell. These effects are integrated over the perimeter and are added to the virtual work expression of the basic element. Furthermore, the constitutive models employed for concrete and steel are based on the results of a recent study and include the confinement and biaxial effects. A 13 degree of freedom (DOF) element with three nodes, which has five DOF per end node and three DOF on the middle node, has been chosen. The quadratic Lagrangian shape functions for axial deformation and the quartic Hermitian shape functions for the transverse directions are used. The model is implemented to analyze several CFT columns under constant concentric axial load and cyclic lateral load. The effect of semi- and perfect bond is investigated and compared with experiments. Good correlation has been found between experimental results and theoretical analyses. The results show that the use of a studded or ribbed steel shell causes greater ultimate strength and higher dissipation of energy than the columns with nonstudded steel shells.

DOI: 10.1061/(ASCE)0733-9399(2002)128:4(428)

CE Database keywords: Tubes; Cyclic loads; Fiber composites; Columns; Steel; Concrete.

Introduction

It is widely recognized that the innovative use of two or more material in structures generally leads to a more efficient and economical system for resisting environmental loads such as seismic forces. In this area, utilizing concrete filled steel tubes (CFTs) is a new idea, which is finding increasing applications in design practice. In spite of excellent advantages, designers rarely utilize CFT systems, since few practical nonlinear frame models have been developed to simulate the important aspects of CFTs. In previous work for simulating cyclic behavior of a CFT column, including recent work by the authors (Golafshani et al. 1999), perfect bond between steel shell and concrete core is assumed. In this paper a comprehensive composite fiber element is implemented to investigate the effect of bond between the concrete core and the steel shell on the inelastic behavior of CFT columns. Until now no practical nonlinear frame models have been developed to simulate the effect of bonding due to both axial and flexural slippage on the behavior of CFT columns. Furthermore, confinement and biaxial effects are also considered in an efficient and simple manner.

Research Need

For an in-depth review of analytical and experimental research on CFT columns the reader is referred to Shams and Saadeghvaziri (1997). In general, there have been many experimental studies of CFT columns, however, the literature is scarce with regard to analytical work. Bond effect is an important characteristic of the response of composite CFT columns, and it is an area where further analytical work can enhance state-of-the-knowledge. It is believed that the bond strength has a significant effect on the behavior of composite members. However, careful examination of numerous test results indicates that there is still uncertainty about the effect of bond strength on the overall response of CFTs. Okamoto and Maeno (1988) investigated the effect of bond strength between the steel tube and concrete core on the behavior of CFT columns filled with high-strength concrete. According to the test results, it was concluded that the bond strength does not have a significant effect on the flexural capacity of CFT columns. One of the major drawbacks of Okamoto's study was that only a limited number of specimens were tested. Thus, the range of variables considered was limited and two or more variables were changed during each test, which makes reaching solid conclusions difficult. On the other hand, the experimental studies carried out in Japan and reported by Yoshioka (1992), and Itoh and Matsumura (1992) indicated that the bending moment capacity would increase by improving the bond between steel tube and concrete core. Shakir-Khalil (1993a,b) also conducted one of the more recent studies, which focused on estimation of bond and strength of

[1]PhD Candidate, Dept. of Civil Engineering, Sharif Univ. of Technology, Azadi Ave., Tehran, Iran.

[2]Professor, Dept. of Civil and Environmental Engineering, New Jersey Institute of Technology, Univ. Heights, Newark, NJ 07102 (corresponding author). E-mail: ala@njit.edu

[3]Assistant Professor, Dept. of Civil Engineering, Sharif Univ. of Technology, Azadi Ave., Tehran, Iran.

Note. Associate Editor: A. Rajah Anandarajah. Discussion open until September 1, 2002. Separate discussions must be submitted for individual papers. To extend the closing date by one month, a written request must be filed with the ASCE Managing Editor. The manuscript for this paper was submitted for review and possible publication on March 24, 2000; approved on February 9, 2001. This paper is part of the ***Journal of Engineering Mechanics***, Vol. 128, No. 4, April 1, 2002. ©ASCE, ISSN 0733-9399/2002/4-428–437/$8.00+$.50 per page.

mechanical shear connectors in a CFT column. Some of the results with regard to bond chracteristics that can be useful to development of analytical tools for response simulation are listed below:

1. In spite of the value of bond strength of 0.4 N/mm^2 that is reported by BS 5400 (1979), the failure load of the control specimens gave an average of 0.8 N/mm^2;
2. For specimens with mechanical shear connectors, the reloading after unloading follows the envelope curve for monotonic loading and repeated loading had no noticeable adverse effect on the failure load of the specimens; and
3. The bond–slip relation under cyclic loading can be evaluated by a bilinear curve that is similar to the stress–strain relation for mild steel.

Thus, there is a need for further analytical work on the effect of bond in order to extrapolate the experimental results beyond the ranges considered and to provide a simple platform for practical application. Therefore, it is necessary to develop an analytical model that is simple and accurate to employ for detailed analysis of the inelastic response of CFT columns including the effect of bond on composite action.

The proposed element is an extension of the element that is used in nonlinear analysis (with small deformations) of composite beams by Ayoub and Filippou (1997) and Salari et al. (1997) in CFT columns. The former work consists of two beam components for the concrete slab and the steel girder, and two concentrated springs at the end nodes for shear connectors. The axial and transverse displacements are interpolated using linear and cubic functions, respectively. In the work by Salari et al. (1997) the same assumptions are considered, but distributed springs for shear connection and quadratic function for axial deformation are used. The use of Hermitian interpolation functions for beam deformation leads to a linear curvature distribution along the beam, which reduces the accuracy of the element in the nonlinear range. Therefore, a higher order shape function is employed. Furthermore, the bond/slip formulation (herein referred to as distributed bond) ensures that the interaction between concrete and steel is represented over the entire contact surface between the two materials. That is, unlike the discrete spring elements used to model the bond, the proposed formulation allows for variations in bonding in both longitudinal and circumferential directions. Thus, although the two methods are as effective under only axial relative slippage, the proposed element can also model differential strain over the height of the cross section. This situation can arise under flexural loading or combined axial and high flexural loading. It should be noted that Hajjar and Gourley (1996, 1997a,b) and Hajjar et al. (1998a,b) have also performed one of the most recent and thorough analytical work on the performance of CFT columns. The original studies (Hajjar 1996, 1997a,b) consist of development of a concentrated plasticity finite element model for CFT members. The more recent work (Hajjar et al. 1998a,b) is a fiber-based distributed plasticity finite element formulation, which is less compact than the concentrated plasticity model. However, it provides more detailed information on behavioral characteristics of a CFT member via the spread of plasticity through the cross section and evaluation of the effect of slip. The element presented in this paper employs the fiber approach, which is a versatile approach in that unlike plasticity models there is no need for prior development and calibration of a cross-section strength interaction. Compared to the Hajjar et al. element (Hajjar et al. 1998a,b) this element also allows for modeling of flexural slip by providing two separate rotational DOFs for concrete and steel. Furthermore, the constitutive models for concrete and steel use the results of a recent study (Shams and Saadeghvaziri 1999) to better represent the confinement and biaxial effects considering the geometric and design factors for the member under consideration.

Solution Strategy and Assumptions

A CFT column consists of two components, i.e., a concrete core and a steel shell around the concrete. The stress transfer between the two components may be increased by the use of inner ribs or a studded shell that can augment the composite action in CFTs. The scope of this research is to develop a practical frame element to consider the bond effect on nonlinear behavior of CFTs under monotonic as well as cyclic loads, which can be used in a general-purpose finite-element program. It is assumed that a distributed bond is maintained between steel shell and concrete core. There are two causes for the slippage between steel shell and concrete core. The first is the difference between elongation of the steel shell and the concrete core, and the second is the difference between curvatures in the cross section for the concrete core and the steel shell. This element is planar, however, extension to a three-dimensional case is straightforward. Furthermore, the formulation can readily be extended to include the torsional DOF to model linear elastic behavior under twist.

In derivation of the formulas, the following assumptions are made:

1. Plane sections of the concrete core and the steel shell before and after bending remain plane, but the angles of rotations are independent;
2. Shear deformations due to the size of the section are negligible;
3. During loading history the shell will not buckle. This assumption has a negligible effect on results for moderate and low aspect ratio;
4. Effects of confinement on concrete and biaxial state of stress in the steel shell are accounted for through the uniaxial material models using recent results (Shams and Saadeghvaziri 1999);
5. The effects of creep and shrinkage are neglected because they have a small influence on the behavior of CFTs (Nakai et al. 1991); and
6. Effects of residual stresses are neglected.

Element Description

The proposed comprehensive composite element consists of three components: two frame elements, one to model the concrete core and another to represent the steel shell, and a distributed bond interface element that represents the relative slippage (see Fig. 1). A 13 DOF combined element that has five DOFs per end node and three DOFs on the middle node has been chosen. Nonlinear behavior of materials on the cross-sectional level leads to a nonlinear relationship between the bending moment and curvature. Because of the complex deformed shape, the conventional cubic polynomial function, which causes a linear relation between moment and curvature, cannot represent the curvature distribution in the element. This problem may be solved by three strategies, i.e., the use of more elements for modeling a member, the use of higher order shape function, or utilizing a flexibility method. For practical proposes, it is better to model a member with only one element. The flexibility method recently developed by Spacone et al. (1996) requires much effort and is not as straightforward as

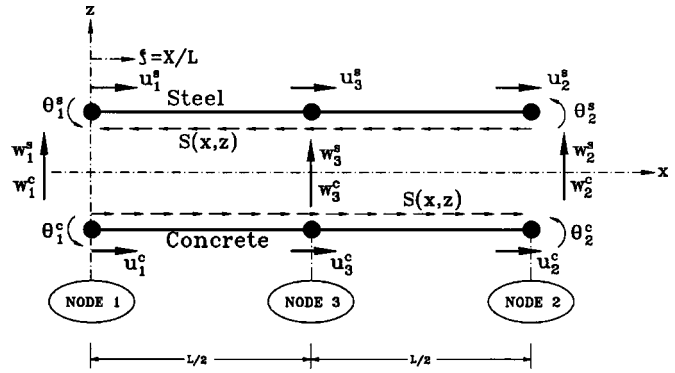

Fig. 1. Degrees of freedoms for proposed element based on Kirchhoff beam theory

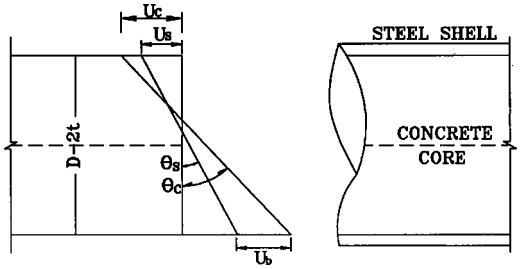

Fig. 2. Kinematics of concrete-filled steel tube column sections (slippage between concrete and steel)

the displacement-based element to compute the resisting forces in the general-purpose finite element program. Therefore, to increase accuracy it was decided to use higher order quartic Hermitian shape function for transverse displacement. The quadratic Lagrangian shape functions for axial deformation are used. Collection of these types of shape functions for transverse and axial deformation leads to cubic order variation of bond at the interface. The explicit forms of these functions for both steel and concrete element are:

$$\mathbf{N}_u^T=\langle 1-3\xi+2\xi^2,-\xi+2\xi^2,4\xi-4\xi^2\rangle \tag{1a}$$

$$\mathbf{N}_w^T=\langle 1-11\xi^2+18\xi^3-8\xi^4,(\xi-4\xi^2+5\xi^3-2\xi^4)L,$$
$$-5\xi^2+14\xi^3-8\xi^4,(\xi^2-3\xi^3+2\xi^4)L,16\xi^2-32\xi^3+16\xi^4\rangle \tag{1b}$$

The nodal displacement vector and corresponding nodal force vector are

$$\mathbf{q}^T=\langle \mathbf{q}_u^c,\mathbf{q}_u^s,\mathbf{q}_w^c,\mathbf{q}_w^s\rangle \tag{2a}$$

$$\mathbf{Q}^T=\langle \mathbf{Q}_u^c,\mathbf{Q}_u^s,\mathbf{Q}_w^c,\mathbf{Q}_w^s\rangle \tag{2b}$$

where

$$\mathbf{q}_u^{cT}=\langle u_1^c,u_2^c,u_3^c\rangle;\quad \mathbf{q}_w^{cT}=\langle w_1^c,\theta_1^c,w_2^c,\theta_2^c,w_3^c\rangle \tag{3a}$$

$$\mathbf{Q}_u^{cT}=\langle U_1^c,U_2^c,U_3^c\rangle;\quad \mathbf{Q}_w^{cT}=\langle W_1,M_1^c,W_2,M_2^c,W_3\rangle \tag{3b}$$

Similar vectors for steel component can be considered using the superscript *s*.

Element Kinematics

The element deformations consist of three components: the displacements of concrete and steel components and the interaction between them, which produces compatibility in displacements. The transverse displacement perpendicular to the axis is the same for concrete and steel components but slippage between the two components produces a distributed bond at the interface. The displacement of two adjacent points in the concrete core and the steel shell are calculated based on axial and flexural deformation of their axis:

$$u_s=\overline{u}_s-z\theta_s;\quad u_c=\overline{u}_c-z\theta_c \tag{4}$$

in which $\overline{u}$ and θ=the axial and rotational deformation of axis. The subscripts *s* and *c*=their values for steel and concrete, respectively. These displacements are shown in Fig. 2. The differences between the two displacements cause the slippage that is evaluated as

$$u_b=\overline{u}_c-\overline{u}_s-z(\theta_c-\theta_s) \tag{5}$$

Governing Equations

In order to include the bond effect, in the virtual work equation the slippage should be integrated around the perimeter and added to the general expression of virtual work from concrete and steel components.

The virtual displacement work equation can be expressed as

$$\delta V=\int_{c+s}\mathbf{D}^T\delta\mathbf{d}\,dx+\int\left[\oint s(x,z)\delta u_b\,d\rho\right]dx-\mathbf{Q}_e^T\delta\mathbf{q}=0 \tag{6}$$

where the bond force denoted by $s(x,z)$ is distributed along the interface and varies with deformation history (see Fig. 1). **D** and **d** are generalized stress and corresponding strain for concrete and steel shell, respectively. They can be expressed as follows:

$$\mathbf{D}=\begin{Bmatrix}N(x)\\M(x)\end{Bmatrix};\quad \mathbf{d}=\begin{Bmatrix}\varepsilon\\\chi\end{Bmatrix}=\begin{Bmatrix}u'(x)+\frac{1}{2}w'^2(x)\\-w''(x)\end{Bmatrix} \tag{7}$$

where the prime symbols indicate the derivative with respect to *x*. $N(x)$ and $M(x)$=the sectional axial force and the sectional bending moment, respectively. The displacement fields $u(x)$ and $w(x)$=the axial and transverse displacements of the beam reference axis, respectively. The derivative of displacement field can be evaluated as

$$\frac{du(x)}{dx}=\mathbf{B}_u\mathbf{q}_u;\quad \frac{dw(x)}{dx}=\mathbf{B}_w\mathbf{q}_w;\quad \chi=-\frac{d^2w(x)}{dx^2}=\mathbf{B}_\chi\mathbf{q}_w \tag{8}$$

and

$$w'^2=\mathbf{q}_w^T\mathbf{A}_w\mathbf{q}_w;\quad \mathbf{A}_w=\mathbf{B}_w^T\mathbf{B}_w \tag{9}$$

so $\mathbf{A}_w$=a symmetric matrix.

With substitution of generalized strain and stress in the expression of Eq. (6), the internal nodal force vector can be expressed as

$$\mathbf{Q}_{ui}^c=\int N^c(x)\mathbf{B}_u^T\,dx+\int f_1(x)\mathbf{N}_u^T\,dx \tag{10a}$$

$$\mathbf{Q}_{ui}^s=\int N^s(x)\mathbf{B}_u^T\,dx-\int f_1(x)\mathbf{N}_u^T\,dx \tag{10b}$$

$$\mathbf{Q}_{wi}^c=\int N^c(x)\mathbf{A}_w\mathbf{q}_w^c\,dx+\int M^c(x)\mathbf{B}_\chi^T\,dx-\int f_2(x)\mathbf{B}_w^T\,dx \tag{10c}$$

$$\mathbf{Q}_{wi}^{s}=\int N^{s}(x)\mathbf{A}_{w}\mathbf{q}_{w}^{s}\,dx+\int M^{s}(x)\mathbf{B}_{\chi}^{T}\,dx+\int f_{2}(x)\mathbf{B}_{w}^{T}\,dx \tag{10d}$$

where $f_1(x)$ and $f_2(x)$ are defined as

$$f_{1}(x)=\oint s(x,z)d\rho;\quad f_{2}(x)=\oint zs(x,z)d\rho \tag{11}$$

where, $d\rho$=a differential length of curved segment at the interface. The tangent stiffness matrix is obtained from differentiation of internal nodal force with respect to nodal displacement

$$\mathbf{K}_{t}=\frac{\partial\mathbf{Q}_{i}}{\partial\mathbf{q}} \tag{12}$$

Therefore the tangent stiffness matrix has the following form:

$$\mathbf{K}_{t}=\begin{bmatrix}\mathbf{Ku}_{C}\mathbf{u}_{C} & \mathbf{Ku}_{C}\mathbf{u}_{S} & \mathbf{Ku}_{C}\mathbf{w}_{C} & \mathbf{Ku}_{C}\mathbf{w}_{S}\\ & \mathbf{Ku}_{S}\mathbf{u}_{S} & \mathbf{Ku}_{S}\mathbf{w}_{C} & \mathbf{Ku}_{S}\mathbf{w}_{S}\\ & & \mathbf{Kw}_{C}\mathbf{w}_{C} & \mathbf{Kw}_{C}\mathbf{w}_{S}\\ \text{SYM.} & & & \mathbf{Kw}_{S}\mathbf{w}_{S}\end{bmatrix} \tag{13}$$

After some manipulation, the stiffness submatrices are given as follows:

$$\mathbf{Ku}_{C}\mathbf{u}_{C}=\int\overline{EA}^{c}\mathbf{B}_{u}^{T}\mathbf{B}_{u}\,dx+\int E_{s}\mathbf{N}_{u}^{T}\mathbf{N}_{u}\,dx \tag{14a}$$

$$\mathbf{Ku}_{C}\mathbf{u}_{S}=-\int E_{s}\mathbf{N}_{u}^{T}\mathbf{N}_{u}\,dx \tag{14b}$$

$$\mathbf{Ku}_{C}\mathbf{w}_{C}=\int\overline{EA}^{c}\mathbf{B}_{u}^{T}\mathbf{q}_{w}^{c^{T}}\mathbf{A}_{w}\,dx-\int\overline{EX}_{s}\mathbf{N}_{u}^{T}\mathbf{B}_{w}\,dx+\int\overline{EX}^{c}\mathbf{B}_{u}^{T}\mathbf{B}_{\chi}\,dx \tag{14c}$$

$$\mathbf{Ku}_{C}\mathbf{w}_{S}=\int\overline{EX}_{s}\mathbf{N}_{u}^{T}\mathbf{B}_{w}\,dx \tag{14d}$$

$$\mathbf{Ku}_{S}\mathbf{u}_{S}=\int\overline{EA}^{s}\mathbf{B}_{u}^{T}\mathbf{B}_{u}\,dx+\int E_{s}\mathbf{N}_{u}^{T}\mathbf{N}_{u}\,dx \tag{14e}$$

$$\mathbf{Ku}_{S}\mathbf{w}_{C}=\int\overline{EX}_{s}\mathbf{N}_{u}^{T}\mathbf{B}_{w}\,dx \tag{14f}$$

$$\mathbf{Ku}_{S}\mathbf{w}_{S}=\int\overline{EA}^{s}\mathbf{B}_{u}^{T}\mathbf{q}_{w}^{s^{T}}\mathbf{A}_{w}\,dx-\int\overline{EX}_{s}\mathbf{N}_{u}^{T}\mathbf{B}_{w}\,dx+\int\overline{EX}^{s}\mathbf{B}_{u}^{T}\mathbf{B}_{\chi}\,dx \tag{14g}$$

$$\mathbf{Kw}_{C}\mathbf{w}_{C}=\int\overline{EA}^{c}\mathbf{A}_{w}\mathbf{q}_{w}^{c}\mathbf{q}_{w}^{c^{T}}\mathbf{A}_{w}\,dx+\int N^{c}(x)\mathbf{A}_{w}\,dx+\int\overline{EI}^{c}\mathbf{B}_{\chi}^{T}\mathbf{B}_{\chi}\,dx+\int\overline{EI}_{s}\mathbf{B}_{w}^{T}\mathbf{B}_{w}\,dx+\int\overline{EX}^{c}\mathbf{B}_{\chi}^{T}\mathbf{q}_{w}^{c^{T}}\mathbf{A}_{w}\,dx+\int\overline{EX}^{c}\mathbf{A}_{w}\mathbf{q}_{w}^{c}\mathbf{B}_{\chi}\,dx \tag{14h}$$

$$\mathbf{Kw}_{c}\mathbf{w}_{s}=-\int\overline{EI}_{s}\mathbf{B}_{w}^{T}\mathbf{B}_{w}\,dx \tag{14i}$$

$$\mathbf{Kw}_{s}\mathbf{w}_{s}=\int\overline{EA}^{s}\mathbf{A}_{w}\mathbf{q}_{w}^{s}\mathbf{q}_{w}^{s^{T}}\mathbf{A}_{w}\,dx+\int N^{s}(x)\mathbf{A}_{w}\,dx+\int\overline{EI}^{s}\mathbf{B}_{\chi}^{T}\mathbf{B}_{\chi}\,dx+\int\overline{EI}_{s}\mathbf{B}_{w}^{T}\mathbf{B}_{w}\,dx+\int\overline{EX}^{s}\mathbf{B}_{\chi}^{T}\mathbf{q}_{w}^{s^{T}}\mathbf{A}_{w}\,dx+\int\overline{EX}^{s}\mathbf{A}_{w}\mathbf{q}_{w}^{s}\mathbf{B}_{\chi}\,dx \tag{14j}$$

where $\overline{EA}$, $\overline{EX}$, and $\overline{EI}$=axial, cross coupling, and flexural stiffness of the section, respectively. They have been evaluated for concrete and steel with superscripts *c* and *s* separately. Their values vary during loading history in inelastic domain and can be estimated with the following integrals over the cross sections:

$$\overline{EA}=\int E_{t}\,dA;\quad\overline{EX}=\int zE_{t}\,dA;\quad\overline{EI}=\int z^{2}E_{t}\,dA \tag{15}$$

where E_t=the tangent modulus for concrete or steel based on nonlinear stress–strain curve during loading history. The bond varies during deformation and is a function of relative displacement of concrete core and steel shell. The relation between bond and slippage is described as

$$\delta s(x,z)=E_{b}\delta u_{b} \tag{16}$$

where E_b=the tangent modulus of the bond–slip relation. The values of E_s, $\overline{EX}_s$ and $\overline{EI}_s$ should be evaluated around the interface of the concrete core and the steel shell as follows:

$$E_{s}=\oint E_{b}\,d\rho;\quad\overline{EX}_{s}=\oint zE_{b}\,d\rho;\quad\overline{EI}_{s}=\oint z^{2}E_{b}\,d\rho \tag{17}$$

The existence of $\mathbf{q}_w$ and $N(x)$ will cause the tangent stiffness matrix $\mathbf{K}_t$ to vary during the load history. The quadratic Lagrangian shape functions are used for axial deformation. In order to ameliorate the membrane locking, the reduced order of integration is used.

As discussed previously, for frames with prismatic members in linear elastic domain, the use of Hermitian polynomials gives an exact solution. Utilizing them corresponds to a linear curvature distribution in the element. Under highly nonlinear behavior this assumption deviates significantly from the actual curvature distribution, giving rise to numerical problems. For the sake of accuracy, more elements must be used in each member. The use of quartic Hermitian shape functions can improve the conditioning of the tangent stiffness matrix. The other benefit of using a higher order shape function is that one can employ a greater number of sample points in the numerical integration, which can better represent the spread of plasticity along the member length. The integration method used is Gauss–Lobatto, which is suitable for beams since it allows for two integration points to coincide with the end sections of the element, where significant inelastic deformations typically take place.

Fiber Element Technique

One of the most promising practical methods for accurate modeling and nonlinear analysis of reinforced concrete beams and columns is the fiber element approach.

The values of $\overline{EA}$, $\overline{EX}$, and $\overline{EI}$ in Eq. (14) at Gauss points must be evaluated during the deformation history. For this purpose, the section is divided into small areas at integration points and the size of these areas depends on the desired accuracy (Fig. 3). The load history for each fiber according to the uniaxial

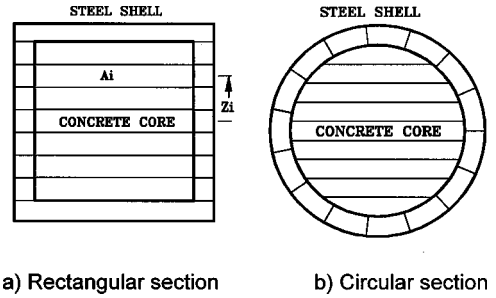

Fig. 3. Fiber representation of concrete-filled steel tube cross sections

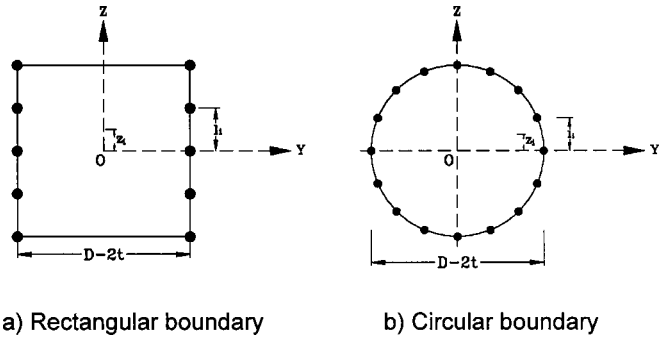

Fig. 4. Discretization of interface to segments

stress–strain relationship should be recorded and this process is completed by a summation for each fiber, i.e.,

$$\overline{EA}=\sum_{i=1}^{n\ \text{fiber}} E_{ti}\cdot A_i;\quad \overline{EX}=\sum_{i=1}^{n\ \text{fiber}} E_{ti}\cdot A_i\cdot Z_i;$$

$$\overline{EI}=\sum_{i=1}^{n\ \text{fiber}} E_{ti}\cdot A_i\cdot Z_i^2 \tag{18}$$

The cyclic uniaxial behaviors of the constituent materials (namely, steel and concrete) are illustrated in the next section.

During loading, the history of the values $f_1(x)$ and $f_2(x)$ as well as E_s, $\overline{EX}_s$, and $\overline{EI}_s$ around the interface should be saved. For this purpose, the interface has been divided into several segments similar to fibers for the concrete and steel shell. Also, the history variables have been saved for each deformation level. Fig. 4 shows the boundary between the steel shell and the concrete core, which has been divided into several segments. Thus, using this segmentation, Eqs. (11) and (18) can be evaluated as follows:

$$f_1(x)=\sum_{i=1}^{n\ \text{seg}} s(x_i,z_i)\Delta\rho_i;\quad f_2(x)=\sum_{i=1}^{n\ \text{seg}} z_i s(x_i,z_i)\cdot\Delta\rho_i \tag{19}$$

$$E_s=\sum_{i=1}^{n\ \text{seg}} E_{bi}\cdot\Delta\rho_i;\quad \overline{EX}_s=\sum_{i=1}^{n\ \text{seg}} z_i E_{bi}\cdot\Delta\rho_i;$$

$$\overline{EI}_s=\sum_{i=1}^{n\ \text{seg}} z_i^2 E_{bi}\cdot\Delta\rho_i \tag{20}$$

As it was mentioned before, experimental results by Shakir-Khalil (1993a,b) indicate that a bilinear perfectly plastic model can be used to model bond–slip relation under cyclic loading. Therefore, perfect plasticity rules are used for bond slip upon loading and unloading.

Material Behavior

The fiber element formulation simplifies the task of material model selection to uniaxial behavior, which is well established to date. Three-dimensional effects on the material behavior can be included in the uniaxial model by appropriate modification of parameters that define the monotonic envelope curve.

Concrete Model

In order to compute the stress in each point due to calculated strain, a material law describing the concrete stress–strain relation under arbitrary cyclic strain histories is needed. The model employed in this study is the one proposed by Mohd Yassin (1994). The monotonic envelope curve of concrete in compression follows the model of Kent and Park (1971) as extended by Scott etal. (1982). The concrete damage considered in this model is in the form of unloading and reloading stiffness degradation for increasing values of the maximum strain. The reduction of the monotonic envelope under cyclic loading is not taken into account in this model. The tensile behavior of the model takes into account tension stiffening and the degradation of the unloading and reloading stiffness for increasing values of the maximum tensile strain after initial cracking. A linear rate of tensile strength reduction is adopted in this model.

It is well known that for concrete confinement has a significant effect on its maximum compressive strength and strain at the maximum stress. However, due to the nature of confinement stress distribution, this effect is not similar for rectangular and circular cross sections (Shams and Saadeghvaziri 1999). Furthermore, for CFT columns other geometric factors such as aspect ratio significantly affect the degree of confinement. Aspect ratio is defined as the ratio of the cross-section diameter (or width) to the thickness of the steel shell. In this study the equations recently proposed by Shams and Saadeghvaziri (1999) for the maximum

Table 1. Specifications of Concrete-Filled Steel Tube Column Specimens

Test	Type of test	N (kN)	N/N_0	Tube dimensions (mm)	L/D	D/t	f'_c (MPa)	Z^c	f_y (MPa)
SI85 (Sakino and Ishibashi 1985)	M^a	140	0.19	SQ100×100×4.25	3.0	24	22.5	1.83	322
ST81 (Sakino and Tomii 1981)	C^b	124	0.20	SQ100×100×4.21	6.0	24	20.4	2.01	296

[a]M=monotonic.

[b]C=cyclic.

[c]Descending slope of stress-strain curve for concrete material (20).

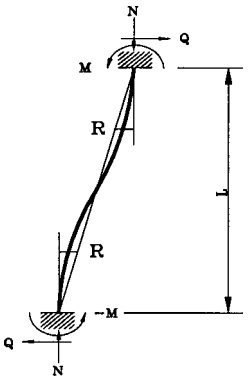

Fig. 5. Overall view of concrete-filled steel tube beam-column experiments

confined strength and corresponding strain are employed. For example, the expression for the maximum confined stress f'_{cc} has the following form:

$$f'_{cc}=f'_c\left(1+\frac{A}{1+\left(\frac{D/t}{B}\right)^{\alpha}}\right) \tag{21}$$

where, f'_c is the uniaxial compressive strength, D/t is the aspect ratio, α is the shape factor, and A and B are empirical parameters expressed in terms of f'_c.

Steel Model

The nonlinear model of Menegotto and Pinto (1973), as modified by Filippou et al. (1983) to also include isotropic strain hardening describes the steel shell stress–strain behavior. In this model elastic and yield asymptotes are assumed to be straight lines, the position of the limiting asymptotes corresponding to the yield surface is assumed to be fixed at all times, and the unloading slope remains constant and equal to the initial slope.

The maximum stresses that the steel tube in CFT columns can sustain depends mainly on the aspect ratio D/t and the length–width ratio L/D. The steel tube under a biaxial state of stress exhibits a lower yield stress. In the case of short columns, the level of decrease in the yield stress depends on the aspect ratio and cross-sectional shape (Shams and Saadeghvaziri 1999). Similar to the concrete material, the expression given by Shams and Saadeghvaziri (1999) is used to consider the biaxial effect on the steel tube.

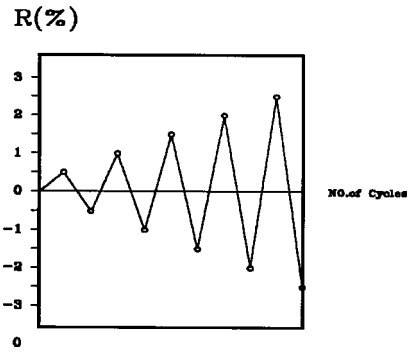

Fig. 6. Loading history

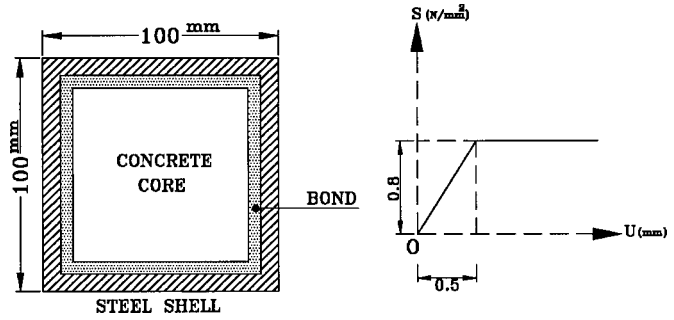

Fig. 7. Description of interface bond element

Illustrative Examples

The proposed beam element is implemented in the nonlinear finite element analysis program (FEAP) developed by Taylor (1998) at the University of California, Berkeley. To demonstrate the versatility of the fiber element, in considering the bond effect in CFTs, a few examples were carried out of which the following examples are reported.

The performance of the proposed composite inelastic fiber element is evaluated by comparing analytical behaviors of two CFT columns to experimental results. Table 1 shows the mechanical properties of the two square sections, which were tested by Sakino and Tomii (1981) under monotonic load, and Sakino and Ishibashi (1985) under cyclic loads.

The test setup is represented in Fig. 5. The axial load is applied first. Then, monotonic or cyclic lateral loads were applied. For simplicity and comparison of results only one cycle of loading in each load level is applied as shown in Fig. 6.

Five Gauss–Lobatto integration points with two elements per specimen are utilized. According to Shakir-Khalil's experiments (Shakir-Khalil 1993a,b) the bond behavior can be modeled by an elastic–perfectly plastic behavior with a yield point of 0.8 N/mm^2 and elastic stiffness of $E_b=1.6$ N/mm^3 (see Fig. 7). Fig. 8 illustrates the correlation between the proposed composite element in three states, i.e., perfect, partial, and without bond between the concrete core and the steel shell versus the experimental results performed by Sakino and Tomii (1981) for monotonic loading. As the degree of bonding increases the strength and energy absorption increases. The three bond types have the same response in linear range ($R<0.25\%$). However after the proportional limit, the response will become different. The experimental results fall between the two cases of without bond and with partial bond

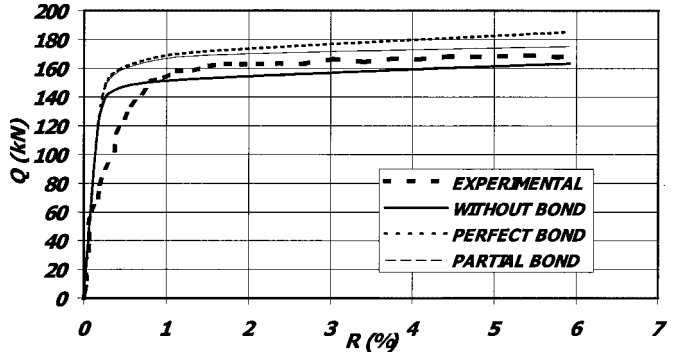

Fig. 8. Comparison of experimental and analytical results under Monotonic loading (Specimen SI85)

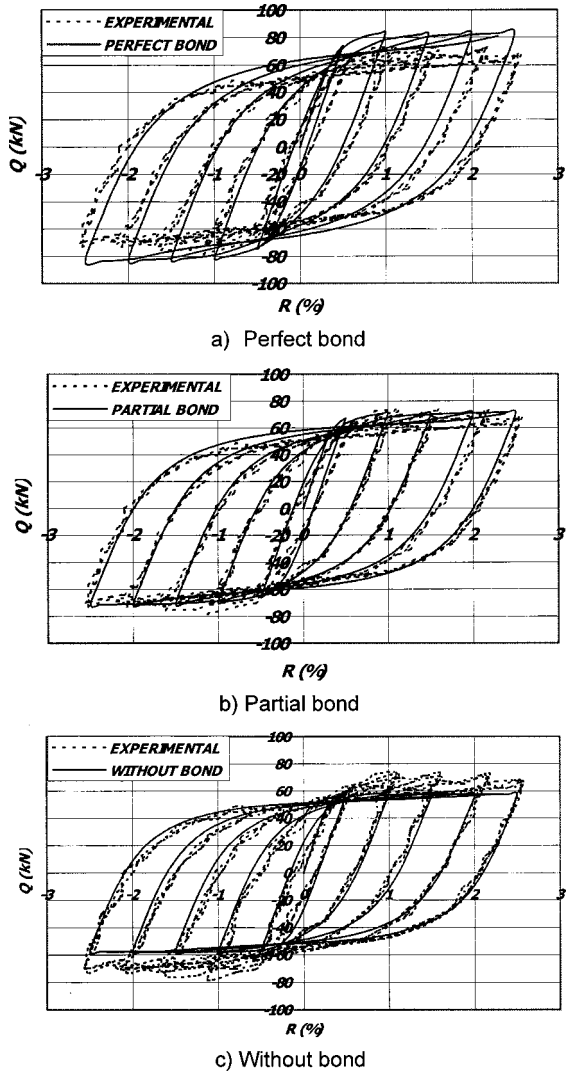

Fig. 9. Comparison of experimental and analytical results under cyclic loading (Specimen ST81)

(with bond strength of 0.8 N/mm^2). The use of the value of 0.4 N/mm^2, which is given in BS 5400 (1979) results in better correlation with experiments. The separation of the steel shell from the concrete core due to local buckling reduces the bonding around the buckled shell. Therefore, on the average bond strength of 0.4 N/mm^2 (as suggested by BS 5400 1979) is more appropriate and gives a better result compared to the bond strength of 0.8 N/mm^2 proposed by Shakir-Khalil (1993a,b).

Fig. 9 illustrates a similar comparison for cyclic loading conducted by Sakino and Ishibashi (1985). It is observed that, in general, there is a good agreement between analytical and experimental results. For monotonic loading, the experimental results show higher stiffness degradation prior to yielding, while under cyclic loading results show higher strength degradation compared to analytical results. This could be due to local buckling, which is not considered in the analysis. The analytical model with partial bond has better correlation to experimental results in comparison with other bond types. The no-bond type model shows lower strength and perfect bond shows higher strength than the experimental results.

It is noted that the compatibility of transverse displacements for concrete and steel components is only satisfied at nodal points

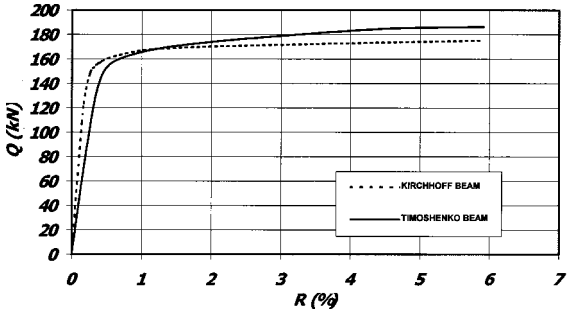

Fig. 10. Comparison of Kirchhoff and Timoshenko formulations for monotonic loading (Specimen SI85)

and some discrepancy can take place within the domain. Due to the major dependency of the transverse displacement field on the nodal points' displacements in the Kirchhoff beam theory, this error is normally negligible. However, to totally eliminate this error one can use the Timoshenko beam theory and separate the transverse and rotational displacement domains. This assumption increases the nodal variables and causes shear locking that can plague the process of solving the nonlinear governing equations. The latter can be resolved by employing selective or reduced integration. In Fig. 10, results are compared for both formulations for column specimen S185 as described in Table 1. In Appendix I, the explicit form of the internal nodal forces and the tangent stiffness are described. As shown in Fig. 10, the results of the two theories under monotonic loading are in close agreement. The Timoshenko formulation shows higher strength in inelastic range and lower stiffness in elastic range when compared to the Kirchhoff formulation of the element. This is because of the use of Lagrangian shape functions instead of Hermitian shape functions. Therefore, by using the Kirchhoff theory not only accurate results are obtained, but also the numerical solution is simpler and more effective.

Conclusions

An inelastic fiber element is developed for practical analysis of composite systems such as CFT columns. The formulation is comprehensive and includes important parameters of nonlinear behavior such as large displacement, material nonlinearity, and bond effect at the interface of the concrete core and steel shell due to both axial and flexural slippage. The proposed comprehensive

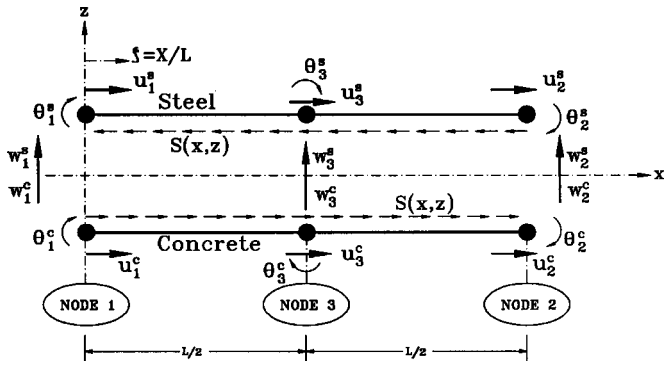

Fig. 11. Degrees of freedom for proposed element based on Timoshenko theory

composite inelastic fiber element proves to be very reliable under monotonic as well as cyclic loading, and it traces the experimental results with good accuracy. It is a versatile element since no predefined phenomenological rules are involved in dictating the overall hysteretic behavior of any cross section. Under the assumption of uniaxial state of stress, only the stress–strain properties of the constituent materials are required to define the properties of any cross section. Furthermore, using the results of a recent study (Shams and Saadeghvaziri 1999) the confinement and biaxial effects are considered. When the local buckling potential is low, e.g., a CFT column with low aspect ratio, the element can trace deformation history under any arbitrary loading. The element enables one to consider the slippage of the concrete core relative to the steel shell in a practical nonlinear analysis.

The results show that the use of studded or ribbed steel shell for enhancement of bond between the concrete core and the steel shell causes greater ultimate strength, and higher dissipation of energy than the columns with nonstudded steel shells. However, it appears that in comparison to composite beams the effect of bonding on ultimate strength is less pronounced. One reason could be due to the fact that unlike composite sections (such as slab-on-girder) there is no eccentricity between the steel and concrete components in CFT columns. Development of this element provides the necessary platform to perform a more detailed investigation of the effect of bond on cyclic performance of CFT columns, and an effective tool for analysis and design of CFT systems.

Appendix I

Fig. 11 shows the collection of nodal variables for the proposed composite CFT element based on Timoshenko beam theory. The nodal degrees of freedom and corresponding nodal forces are:

$$\mathbf{q}^T=\langle \mathbf{q}_u^c,\mathbf{q}_u^s,\mathbf{q}_w^c,\mathbf{q}_w^s,\mathbf{q}_\theta^c,\mathbf{q}_\theta^s\rangle \tag{22a}$$

$$\mathbf{Q}^T=\langle \mathbf{Q}_u^c,\mathbf{Q}_u^s,\mathbf{Q}_w^c,\mathbf{Q}_w^s,\mathbf{Q}_\theta^c,\mathbf{Q}_\theta^s\rangle \tag{22b}$$

where

$$\mathbf{q}_u^{c^T}=\langle u_1^c,u_2^c,u_3^c\rangle;\quad \mathbf{q}_w^{c^T}=\langle w_1^c,w_2^c,w_3^c\rangle;\quad \mathbf{q}_\theta^{c^T}=\langle \theta_1^c,\theta_2^c,\theta_3^e\rangle \tag{23a}$$

$$\mathbf{Q}_u^{c^T}=\langle U_1^c,U_2^c,U_3^c\rangle;\quad \mathbf{Q}_\theta^{c^T}=\langle M_1^c,M_2^c,M_3^c\rangle;$$
$$\mathbf{Q}_w^{c^T}=\langle W_1,W_2,W_3\rangle \tag{23b}$$

Similar vectors for steel component can be considered using the superscript *s*. The equivalent internal nodal forces can be obtained as

$$\mathbf{Q}_{ui}^c=\int N^c(x)\mathbf{B}_u^T\,dx+\int f_1(x)\mathbf{N}_u^T\,dx \tag{24a}$$

$$\mathbf{Q}_{ui}^s=\int N^s(x)\mathbf{B}_u^T\,dx-\int f_1(x)\mathbf{N}_u^T\,dx \tag{24b}$$

$$\mathbf{Q}_{wi}^c=\int N^c(x)\mathbf{A}_w\mathbf{q}_w^c\,dx+\int Q^c(x)\mathbf{B}_w^T\,dx \tag{24c}$$

$$\mathbf{Q}_{wi}^s=\int N^s(x)\mathbf{A}_w\mathbf{q}_w^s\,dx+\int Q^s(x)\mathbf{B}_w^T\,dx \tag{24d}$$

$$\mathbf{Q}_{\theta_i}^c=\int M^c(x)\mathbf{B}_\theta^T\,dx+\int Q^c(x)\mathbf{N}_\theta^T\,dx+\int f_2(x)\mathbf{N}_\theta^T\,dx \tag{24e}$$

$$\mathbf{Q}_{\theta_i}^s=\int M^s(x)\mathbf{B}_\theta^T\,dx+\int Q^s(x)\mathbf{N}_\theta^T\,dx-\int f_2(x)\mathbf{N}_\theta^T\,dx \tag{24f}$$

and the tangent stiffness matrices are

$$\mathbf{K}_t=\begin{bmatrix}\mathbf{Ku}_C\mathbf{u}_C & \mathbf{Ku}_C\mathbf{u}_S & \mathbf{Ku}_C\mathbf{w}_C & \mathbf{0} & \mathbf{Ku}_C\theta_C & \mathbf{Ku}_C\theta_S\\ & \mathbf{Ku}_S\mathbf{u}_S & \mathbf{0} & \mathbf{Ku}_S\mathbf{w}_S & \mathbf{Ku}_S\theta_C & \mathbf{Ku}_S\theta_S\\ & & \mathbf{Kw}_C\mathbf{w}_C & \mathbf{0} & \mathbf{Kw}_C\theta_C & \mathbf{0}\\ & & & \mathbf{Kw}_S\mathbf{w}_S & \mathbf{0} & \mathbf{Kw}_S\theta_S\\ & & & & \mathbf{K}\theta_C\theta_C & \mathbf{K}\theta_C\theta_S\\ \mathbf{SYM}. & & & & & \mathbf{K}\theta_S\theta_S\end{bmatrix} \tag{25}$$

where

$$\mathbf{Ku}_C\mathbf{u}_C=\int \overline{EA}^c\mathbf{B}_u^T\mathbf{B}_u\,dx+\int E_s\mathbf{N}_u^T\mathbf{N}_u\,dx \tag{26a}$$

$$\mathbf{Ku}_C\mathbf{u}_S=-\int E_s\mathbf{N}_u^T\mathbf{N}_u\,dx \tag{26b}$$

$$\mathbf{Ku}_C\mathbf{w}_C=\int \overline{EA}^c\mathbf{B}_u^T\mathbf{q}_w^{c^T}\mathbf{A}_w\,dx \tag{26c}$$

$$\mathbf{Ku}_C\boldsymbol{\theta}_C=\int \overline{EX}^c\mathbf{B}_u^T\mathbf{B}_\theta\,dx+\int \overline{EX}_s\mathbf{N}_u^T\mathbf{N}_\theta\,dx \tag{26d}$$

$$\mathbf{Ku}_C\boldsymbol{\theta}_S=-\int \overline{EX}_s\mathbf{N}_u^T\mathbf{N}_\theta\,dx \tag{26e}$$

$$\mathbf{Ku}_S\mathbf{u}_S=\int \overline{EA}^s\mathbf{B}_u^T\mathbf{B}_u\,dx+\int E_s\mathbf{N}_u^T\mathbf{N}_u\,dx \tag{26f}$$

$$\mathbf{Ku}_S\mathbf{w}_S=\int \overline{EA}^s\mathbf{B}_u^T\mathbf{q}_w^{s^T}\mathbf{A}_w\,dx \tag{26g}$$

$$\mathbf{Ku}_S\boldsymbol{\theta}_C=-\int \overline{EX}^s\mathbf{N}_u^T\mathbf{N}_\theta\,dx \tag{26h}$$

$$\mathbf{Ku}_S\boldsymbol{\theta}_S=\int \overline{EX}_s\mathbf{B}_u^T\mathbf{B}_\theta\,dx+\int \overline{EX}^s\mathbf{N}_u^T\mathbf{N}_\theta\,dx \tag{26i}$$

$$\mathbf{Kw}_C\mathbf{w}_C=\int \overline{EA}^c\mathbf{A}_w\mathbf{q}_w^c\mathbf{q}_w^{c^T}\mathbf{A}_w\,dx+\int N^c(x)\mathbf{A}_w\,dx+\int \overline{GA}^c\mathbf{B}_w^T\mathbf{B}_w\,dx \tag{26j}$$

$$\mathbf{Kw}_C\boldsymbol{\theta}_C=\int \overline{EX}^c\mathbf{A}_w\mathbf{q}_w^c\mathbf{B}_\theta\,dx+\int \overline{GA}^c\mathbf{B}_w^T\mathbf{N}_\theta\,dx \tag{26k}$$

$$\mathbf{Kw}_S\mathbf{w}_S=\int \overline{EA}^s\mathbf{A}_w\mathbf{q}_w^s\mathbf{q}_w^{s^T}\mathbf{A}_w\,dx+\int N^s(x)\mathbf{A}_w\,dx+\int \overline{GA}^s\mathbf{B}_w^T\mathbf{B}_w\,dx \tag{26l}$$

$$\mathbf{K}w_S\theta_S = \int \overline{EX}^s \mathbf{A}_w \mathbf{q}_w^s \mathbf{B}_\theta \, dx + \int \overline{GA}^s \mathbf{B}_w^T \mathbf{N}_\theta \, dx \quad (26m)$$

$$\mathbf{K}\theta_C\theta_C = \int \overline{EI}^c \mathbf{B}_\theta^T \mathbf{B}_\theta \, dx + \int \overline{GA}^c \mathbf{N}_\theta^T \mathbf{N}_\theta \, dx + \int \overline{EI}_s \mathbf{N}_\theta^T \mathbf{N}_\theta \, dx \quad (26n)$$

$$\mathbf{K}\theta_C\theta_S = -\int \overline{EI}_s \mathbf{N}_\theta^T \mathbf{N}_\theta \, dx \quad (26o)$$

$$\mathbf{K}\theta_S\theta_S = \int \overline{EI}^s \mathbf{B}_\theta^T \mathbf{B}_\theta \, dx + \int \overline{GA}^s \mathbf{N}_\theta^T \mathbf{N}_\theta \, dx + \int \overline{EI}_s \mathbf{N}_\theta^T \mathbf{N}_\theta \, dx \quad (26p)$$

where the internal axial, flexural, moment, and shear and corresponding stiffness ($\overline{EA}$, $\overline{EI}$, $\overline{EX}$, and $\overline{GA}$, which=the axial, flexural, cross coupling, and shear stiffness, respectively, of the section) have been evaluated for concrete and steel with superscript *c* and *s* separately.

All of the above parameters except $\overline{GA}$ depend on the nonlinear history of the material section and can be estimated as before. It is assumed in this research that the shear deformation is elastic during the loading history. For a rectangular section, a modifying coefficient of 5/6 is used to estimate the shear stiffness of the cross section.

Notation

The following symbols are used in this paper:

$\mathbf{B}_u, \mathbf{B}_w, \mathbf{B}_\chi, \mathbf{B}_\theta$ = strain matrices corresponding to axial, transverse, curvature, and rotation displacement;
D = depth of section;
$\mathbf{D}$ = generalized stress;
$d\rho$ = differential segment in peripheral direction at interface;
$\mathbf{d}$ = generalized strain;
E_s = tangent modulus of bond–slip relation;
E_t = tangent modulus for concrete or steel;
$\overline{EA}$, $\overline{EX}$, $\overline{EI}$, $\overline{GA}$ = axial, cross coupling, flexural, and shear stiffness of cross section;
f'_{cc}, f'_c = confined and unconfined compressive strength of concrete core;
$\mathbf{K}_t$ = tangent stiffness matrix;
L = element's length;
$\mathbf{N}_u$, $\mathbf{N}_w$, $\mathbf{N}_\theta$ = shape functions for axial, transverse, and rotation deformation;
$N(x)$, $M(x)$, $Q(x)$ = axial, moment, and shear sectional forces;
$\mathbf{Q}$ = nodal force vector;
$\mathbf{Q}_u, \mathbf{Q}_w, \mathbf{Q}_\theta$ = nodal force vector corresponding to axial, transverse, and rotation;
$\mathbf{q}$ = nodal displacement vector;
$\mathbf{q}_u$, $\mathbf{q}_w$, $\mathbf{q}_\theta$ = nodal displacement vector corresponding to axial, transverse, and rotation;
$s(x,z)$ = bond at (x,z) coordinate;
t = thickness of steel shell;
V = work of virtual displacements;
ε = axial strain of axis;
ξ = nondimensional coordinate; and
χ = curvature.

References

Ayoub, A., and Filippou, F. C. (1997). "A model for composite steel-concrete girders under cyclic loading." *Proc., ASCE Struct. Congr. XV*, Vol. 1, L. Kempner Jr. and C. B. Brown, eds., ASCE, New York, 721–725.

BS 5400 Steel, Concrete and Composite Bridges. (1979). *Code of practice for design of composite bridges*, British Standards Institution, London.

Filippou, F. C., Popov, E. P., and Bertero, V. V. (1993). "Effects of bond deterioration on hysteretic behavior of reinforced concrete joints." *EERC Rep. No. 83/19*, Earthquake Engineering Research Center, Univ. of California, Berkeley, Calif.

Golafshani, A. A., Aval, B., B., and Saadeghvaziri, M. A. (1999). "An inelastic fiber element for analysis of concrete-filled steel tubes under cyclic loads." *Proc., 24th Conf. on our World in Concrete & Structures*, Singapore.

Hajjar, J. F., and Gourley, B. C. (1996). "Representation of concrete-filled steel tube cross-section strength." *J. Struct. Eng.*, 122(11), 1327–1336.

Hajjar, J. F., and Gourley, B. C. (1997a). "A cyclic nonlinear model for concrete-filled tubes." J. Struct. Eng., 123(6).

Hajjar, J. F., and Gourley, B. C. (1997). "Verification." *J. Struct. Eng.*, 123(6), 736–754.

Hajjar, J. F., Molodan, A., and Schiller, P. H. (1998a). "A distributed plasticity model for cyclic analysis of concrete-filled steel tube beam-columns and composite frames." *Eng. Struct.*, 20(4–6), 398–412.

Hajjar, J. F., Schiller, P. H., and Molodan, A. (1998b). "A distributed plasticity model for concrete-filled steel tube beam-columns with interlayer slip." *Eng. Struct.*, 20(8), 663–676.

Itoh, S., and Matsumura, H. (1992). "Steel-concrete composite structure using steel tube with ribs." *Proc., US–Japan Workshop Composites and Structures*, Berkeley, Calif., 136–139.

Kent, D. C., and Park, R. (1971). "Flexural members with confined concrete." *J. Struct. Div., ASCE*, 97(ST7), 1964–1990.

Menegotto, M., and Pinto, P. E. (1973). "Method of analysis for cyclically loaded reinforced concrete plane frames including changes in geometry and non-elastic behavior of elements under combined normal force and bending." *Proc., IABSE Symp. on Resistance and Ultimate Deformability of Structures Acted on by Well Defined Repeated Loads*, Lisbon, Portugal.

Mohd Yassin, M. Y. (1994). "Nonlinear analysis of prestressed concrete structures under monotonic and cyclic loads." PhD dissertation, Univ. of California, Berkeley, Calif.

Nakai, H., Kurita, A., and Ichinose, L. H. (1991). "An experimental study on creep of concrete filled steel pipes." *Proc., 3rd Int. Conf. Steel-Concrete Compos. Struct.*, M. Wakabayashi, ed., Assn. for Int. Cooperation and Res. in Steel-Concrete Composite Struct., Fukuoka, Japan, 55–65.

Okamato, T., and Maeno, T. (1988). "Experimental study on rectangular steel tube columns infilled with ultra high strength concrete hardened by centrifugal force." *Proc., Annual Meeting of AIJ*, Chiba, Japan, 1359.

Sakino, K., and Ishibashi, H. (1985). "Experimental studies on concrete filled square steel tubular short columns subjected to cyclic shearing force and constant axial force." *Trans. Architectural Institute Jpn. (Tokyo)*, 353, 81–89.

Sakino, K., and Tomii, M. (1981). "Hysteretic behavior of concrete filled square shell tubular beam-columns failed in flexure." *Trans. Jpn. Concrete Institute (Tokyo)*, 3, 439–446.

Salari, M. R., Spacone, E., Shing, P. B., and Frangopol, D. M. (1997). "Behavior of composite structures under cyclic loading." *Proc., ASCE Struct. Congr. XV*, Vol. 1, L. Kempner Jr. and C. B. Brown, eds., ASCE, New York, 731–735.

Scott, B. D., Park, R., and Priestley, M. J. N. (1982). "Stress–strain behavior of concrete confined by overlapping hoops at low and high strain rates." *ACI Struct. J.*, 79, 13–27.

Shakir-Khalil, H. (1993a). ''Pushout strength of concrete-filled steel-hollow sections.'' *Struct. Eng.*, 71(13), 230–233.
Shakir-Khalil, H. (1993b). ''Resistance of concrete-filled steel tubes pushout force.'' *Struct. Eng.*, 71(13), 234–243.
Shams, M., and Saadeghvaziri, M. Ala. (1997). ''The state-of-the-art of concrete-filled steel tubular columns.'' ACI Struct. J., 94(5).
Shams, M., and Saadeghvaziri, M. Ala. (1999). ''Nonlinear response of CFT columns under axial load.'' ACI Struct. J., 96(6).
Spacone, E., Filippou, F. C., and Taucer, F. F. (1996). ''Fiber beam-column model for nonlinear analysis of R/C Frames. I: Formulation.'' *Earthquake Eng. Struct. Dyn.*, 25(7), 711–725.
Taylor, R. L. (1998). ''FEAP—A Finite Element Analysis Program.'' Dept. of Civil Engineering, Univ. of California, Berkeley, Calif.
Yoshioka, Y. (1992). ''State of art of composite steel tube and concrete structures in Japan.'' *Proc., US–Japan Workshop, Composite and Hybrid Structures*, Berkeley, Calif., 119–135.